Journal of Physics and Chemistry of Solids 213 (2026) 113621

Contents lists available at ScienceDirect

Journal of Physics and Chemistry of Solids

journal homepage: www.elsevier.com/locate/jpcs

Phase transitions, polar and magnetic orderings in perovskites of the $BiFeO_3$–$BiCrO_3$ series

A.N. Salak [a,*], J.P. Cardoso [a], D.D. Khalyavin [b], A.V. Pushkarev [1], Yu.V. Radyush [1], N.M. Olekhnovich [1], E.L. Fertman [c], A.V. Fedorchenko [c], D. Sokol [d], E. Palaimienė [e], J. Banys [e], S. Salamon [f], H. Wende [f], A. Feher [g], E. Čižmár [g,**]

[a] Department of Materials and Ceramics Engineering and CICECO – Aveiro Institute of Materials, University of Aveiro, 3810-193, Aveiro, Portugal
[b] ISIS Facility, Rutherford Appleton Laboratory, Chilton, Didcot, Oxfordshire, OX11 0QX, UK
[c] B. Verkin Institute for Low Temperature Physics and Engineering of NAS, 61103, Kharkov, Ukraine
[d] Faculty of Chemistry and Geosciences, Vilnius University, LT-03225, Vilnius, Lithuania
[e] Faculty of Physics, Institute of Applied Electrodynamics and Telecommunications, Vilnius University, LT-10257, Vilnius, Lithuania
[f] Faculty of Physics and CENIDE – Center for Nanointegration Duisburg-Essen, University of Duisburg-Essen, 47057, Duisburg, Germany
[g] Institute of Physics, Faculty of Sciences, P. J. Safarik University, 041 54, Košice, Slovakia

ARTICLE INFO

Keywords:
High-pressure synthesis
Oxygen octahedral tilting
Conversion polymorphism
Dielectric dispersion
G-type antiferromagnetic

ABSTRACT

The high-pressure stabilized perovskite phases of the $BiFe_{1-x}Cr_xO_3$ solid solutions ($0 \leq x \leq 1$) were studied in respect of their stability at ambient pressure, phase coexistence and phase transitions as well as dielectric properties and magnetic behaviour. The as prepared phases with $x \leq 0.50$ are the rhombohedral *R3c*. In the compositional range of $0.55 \leq x \leq 0.90$, the solid solutions are the antipolar orthorhombic *Pnma*, while the monoclinic *C2/c* phase is formed when $x \geq 0.95$. Upon heating, all the studied compositions exhibit structural transition into a high-temperature non-polar orthorhombic *Pnma* modification. The transition is reversible; the only exception is the case of the solid solution with $x = 0.55$, which transforms to the two-phase mixture (*R3c* + antipolar *Pnma*) upon cooling. The $BiFe_{1-x}Cr_xO_3$ ceramics demonstrate high dielectric constant yet a relatively high dielectric loss, which grows with increasing temperature. Dielectric dispersion likely caused by ferroelectric domain was observed and activation energy was estimated as a function of chromium content. The composition with $x = 0.95$ shows a spin re-orientation transition, which is suppressed when $x \leq 0.90$. In the Cr-rich compositional range, a magnetization reversal effect below the Néel temperature was observed.

1. Introduction

Bismuth-containing perovskites represent an intriguing class of materials with fascinating physical properties associated with stereochemical activity of $6s^2$ lone pair electrons of Bi^{3+}. This electronic instability often results in ferro- and antiferroelectric order, piezoelectricity and multiferroicity. For instance, the only known multiferroic, which merges a proper ferroelectricity and magnetism at room temperature is $BiFeO_3$. The trigonal crystal structure of this perovskite involves polar atomic displacements and anti-phase tilting of octahedra about the polar axis. The structural distortions have a strong impact on the magnetic ground state. The dominant exchange interactions are antiferromagnetic, stabilising the so-called G-type antiferromagnetic structure, where each spin is antiparallel to its neighbours. The octahedral tilting and the polar structural distortions impose antisymmetric exchange interactions promoting ferromagnetic canting (weak ferromagnetism) and modulated state, respectively. The presence of the ferromagnetic component is particularly desirable for an efficient cross-coupling between the electronic and magnetic subsystems. However, the part of antisymmetric exchange associated with the polar distortions stabilises an incommensurate cycloidal structure, which averages the weak ferromagnetic component to zero [1,2]. To suppress the modulation, such approaches as chemical modification, thin film manufacturing, domain engineering were used [3–5]. Among them,

* Corresponding author.
** Corresponding author.
E-mail addresses: salak@ua.pt (A.N. Salak), erik.cizmar@upjs.sk (E. Čižmár).
[1] Independent researchers.

https://doi.org/10.1016/j.jpcs.2026.113621
Received 20 October 2025; Received in revised form 19 February 2026; Accepted 20 February 2026
Available online 23 February 2026

atomic substitutions represent the simplest & controllable one. Substitutions in the *A*-site of $BiFeO_3$ are the most reported, particularly the cases of replacement of Bi^{3+} with rare-earth cations [4,5]. In contrary, *B*-site substitutions have scarcely been studied, mainly because of a very small replacement rate that can be achieved using the conventional synthesis routes. *B*-site substitutions in bismuth ferrite are of particular interest, especially when recurring to magnetic cations [4,6]. A cooperation between magnetic cations in the *B*-site and the resultant polarization from bismuth's lone pair of valent electrons may lead to interesting and novel magnetic structures. The system with Fe^{3+}-to-Mn^{3+} substitution, $BiFe_{1-y}Mn_yO_3$, is the most studied both experimentally and theoretically [7–11]. Unlike bismuth ferrite, synthesis of bulk $BiMnO_3$ requires high-pressure to stabilize this composition in perovskite structure [12]. Nonetheless, the conventional ceramic processing route is sufficient to produce single-phase perovskite compositions with the manganese substitution rate up to 30 mol% [13,14]. In this range, the crystal structure of the solid solutions was found to remain the same as that of the parent bismuth ferrite, namely the rhombohedral *R*3*c*. By processing the whole series under high-pressure, the $BiFe_{1-y}Mn_yO_3$ compositions with the manganese content up to 10 mol % crystallize in the *R*3*c* structure, while for $0.15 \leq y \leq 0.60$ the structure is antipolar orthorhombic, *Pnma* [7,15]. For compositions with *y* corresponding to 80 mol% of Mn and higher, the structure is monoclinic *C*2/*c*, as that of undoped $BiMnO_3$ [7,16]. Upon annealing, the orthorhombic phase with the compositions from the range of $0.15 \leq y \leq 0.30$ transforms *irreversibly* into the rhombohedral *R*3*c* one [15]. For the remaining compositional range, the heating-cooling cycles are accompanied by *reversible* transformations into/from the high-temperature non-polar orthorhombic phase, which is also *Pnma* but with different metric with respect to the primitive perovskite unit cell [7]. The compositional sequence of crystal structures observed in unannealed $BiFeO_3$–$BiMnO_3$ is the same as that in as-prepared $BiFeO_3$–$BiScO_3$ series synthesized under high pressure [17]. However, annealing behaviour of these two systems is rather different. Unlike $BiFeO_3$–$BiMnO_3$, the scandium-containing system has three compositional ranges where *irreversible* temperature-induced transitions occur originating new structural phases, which are not present in the phase diagram of the as-prepared compositions [18–20]. This phenomenon, known as *conversion polymorphism* [20], was shown to be a general mechanism, deserving detailed study and exploration in other high-pressure stabilized perovskites.

The same as $BiMnO_3$, $BiCrO_3$ perovskite compound has been first high-pressure synthesized and characterized by Sugawara to be monoclinic *C*2/*c* [12]. However, unlike the former (which is ferromagnetic), bismuth chromate exhibits a G-type antiferromagnetic (AFM) structure below $T_N = 114$ K, with a weak ferromagnetic (FM) component [21,22]. $BiCrO_3$ itself and $BiCrO_3$-based composition have been reported to exhibit a spin-reorientation transition below their Néel temperature [21–25]. Only ten years ago solid solutions of the $BiFeO_3$–$BiCrO_3$ system were much less studied than those of the $BiFeO_3$–$BiMnO_3$ series, likely due to the small solubility (about 10 mol.%) of bismuth chromate in bismuth ferrite at ambient pressure [26]. However, in 2018, McBride et al. reported a synthesis of almost stochiometric $BiFe_{0.5}Cr_{0.5}O_3$ using a new *near-ambient-pressure* solid-state method [27]. They confirmed that crystal structure of the obtained material is rhombohedral *R*3*c* as that earlier found in the $BiFe_{0.5}Cr_{0.5}O_3$ ceramics synthesized under high pressure [28]. Over the last decade, an interest to the $BiFeO_3$–$BiCrO_3$ system has suddenly increased [29–34]. High-pressure synthesis was used to prepare the rhombohedral $BiFe_{1-x}Cr_xO_3$ compositions with $x =$ 0.05, 0.10, and 0.20, which were then studied using Mössbauer spectroscopy [29,31]. Inspired by first principles theoretical predictions of high-polarization & large magnetic moment in rhombohedral $BiFe_{0.5}Cr_{0.5}O_3$ [35], Wu et al. studied in detail structural, magnetic, dielectric and optical properties of this equimolar solid solution of $BiFeO_3$ and $BiCrO_3$ [36]. A compositional range of orthorhombic structure was then found in the high-pressure stabilized perovskites of the $BiFe_{1-x}Cr_xO_3$ system ($x > 0.5$) [30] The borders of the orthorhombic phase, with the ranges of the rhombohedral ($BiFeO_3$-rich) phase and the monoclinic ($BiCrO_3$-rich) one, were roughly estimated to be at 0.50-0.60 and 0.85-0.95, respectively. Then the temperature dependence of the $BiFe_{1-x}Cr_xO_3$ magnetic transition temperature was reported [32].Very recently, Belik reported high-pressure synthesis, annealing behaviour, crystal structure and magnetic properties of ceramic samples from the Cr-rich side of bulk $BiFe_{1-x}Cr_xO_3$ solid solutions ($0.6 \leq x \leq 0.9$) [37]. In the compositions with *x* between 0.1 and 0.3, he revealed an annealing-stimulated irreversible transformation (*conversion polymorphism*) from the *C*2/*c* phase to the *Pnma* one.

Here we report on results of systematic study of the structure, dielectric and magnetic properties of the high-pressure stabilized perovskite phases in the entire compositional range of the $BiFe_{1-x}Cr_xO_3$ solid solutions ($0 \leq x \leq 1$) as well as their behaviour upon annealing.

2. Experimental

Ceramics of the $BiFe_{1-x}Cr_xO_3$ series ($x = 0.10$, 0.20, 0.25, 0.30, 0.40, 0.50, 0.55, 0.60, 0.70, 0.75, 0.80, 0.85, 0.90 and 0.95) were synthesized under high-pressure from the precursors prepared either by means of a solid-state reaction of the oxide mixture or using a sol-gel route. Details of the precursor preparation can be found in the Supplementary Material.

The powders were pressed into pellets of 4.5 mm in diameter and about 4 mm height and then processed at 4 GPa using an anvil press DO-138A equipped with a Bridgman-type apparatus. The high-pressure synthesis temperature was 1570-1670 K (depending on composition); the dwell time did not exceed 5 min. Then a container with sample was quenched to room temperature followed by fast release of pressure. Such a procedure ensures keeping the synthesized materials as a metastable phase at ambient conditions. It should be noted, however, that this feature of high-pressure synthesis results in huge inhomogeneous stress and defects in the obtained ceramics, which usually make difficult their poling and measurements in high electric field.

Phase analysis and the crystal structure characterization were done *via* X-ray diffraction (XRD) on the powders obtained from the as-prepared ceramics. XRD measurements were performed using a PANalytical X'Pert MPD PRO diffractometer (Ni filtered Cu Kα radiation) with an exposition of about 2 s per 0.02° step over a 2-theta range of 10-90°. The structural parameters for the end member of the series, $BiCrO_3$, were taken from the neutron diffraction data, collected on WISH diffractometer (ISIS Facility, UK) [25]. *In situ* temperature XRD studies were conducted in an Anton Paar HTK 16 N chamber upon both heating and cooling. First thermal cycle was done between 300 and 870 K with a step of 50 K to estimate the ranges of possible structural transformations, phase coexistence and decomposition of the high-pressure stabilized compositions. Then the measurements were repeated with maximum temperature well below the stability limit with a step of 10 K in vicinity of phase transitions detected in a course of previous cycle. The obtained XRD data were refined by the Rietveld method using the FULLPROF suite [38].

The microstructure of the ceramics was studied using a Hitachi S-4100 scanning electron microscope (SEM) operating at 25 kV. The grain size was measured on a fractured surface, on at least 100 grains, with the use of the software ImageJ.

The dielectric response of the ceramics was measured in the range of 200-530 K on cooling with a rate of 1 K/min. Silver paste electrodes were deposited on the samples for electrical measurements. The measurements were performed in two frequency ranges, namely between 20 Hz and 1 MHz, and from 1 MHz to 1 GHz. Correspondingly, an LCR meter HP-4284A and a vector network analyser Agilent 8714 ET in a coaxial line were used.

Magnetic properties of the samples were measured in the range of 5-400 K using the vibrating sample magnetometry (VSM) option of a Quantum Design PPMS DynaCool system (University of Duisburg-Essen)

and a Quantum Design MPMS3 magnetometer (P.J. Šafárik University). Temperature dependent data were collected both in zero-field-cooled (ZFC) and field cooled (FC) modes in the applied field 100 Oe. Magnetic hysteresis loops were measured at different temperatures in magnetic field up to 70 kOe. The temperature dependence of the AC susceptibility was measured for selected excitation frequencies for selected concentrations (with high x values).

3. Results and discussion

3.1. Phase content and crystal structure

The as-prepared samples of the $BiFe_{1-x}Cr_xO_3$ perovskite solid solutions were first characterized using XRD at room temperature. The ranges of three different structural phases were observed with increasing Cr content. The most representative fragments of the XRD patterns of the compositions corresponding to these phases are demonstrated in Fig. 1. The structures were identified from the relative intensities and the splitting observed. Two boundaries separating the ranges of the rhombohedral *R3c* phase ($0 \le x \le 0.50$) the orthorhombic *Pnma* ($0.55 \le x \le 0.90$), and the monoclinic *C2/c* one ($0.95 \le x \le 1$), respectively, were found. In contrast with the data recently reported by Belik [37], no phase coexistence in any compositional ranges studied was detected.

To facilitate comparison of lattice distortions of the prototype cubic perovskite structure, associated with macroscopic strains, the unit cell parameters obtained from the refinement of the identified structural phases were converted into the pseudocubic cell using the following relations: $\boldsymbol{a_h} = -\boldsymbol{a_p} + \boldsymbol{b_p}$, $\boldsymbol{b_h} = -\boldsymbol{b_p} + \boldsymbol{c_p}$, $\boldsymbol{c_h} = 2\boldsymbol{a_p} + 2\boldsymbol{b_p} + 2\boldsymbol{c_p}$ (for the *R3c* phase); $\boldsymbol{a_o} = \boldsymbol{a_p} + \boldsymbol{c_p}$, $\boldsymbol{b_o} = 4\boldsymbol{b_p}$, $\boldsymbol{c_o} = -2\boldsymbol{a_p} + 2\boldsymbol{c_p}$ (*Pnma*) and $\boldsymbol{a_m} = 2\boldsymbol{a_p} + \boldsymbol{b_p} + \boldsymbol{c_p}$, $\boldsymbol{b_m} = \boldsymbol{b_p} - \boldsymbol{c_p}$, $\boldsymbol{c_m} = -2\boldsymbol{a_p} + \boldsymbol{b_p} + \boldsymbol{c_p}$ (*C2/c*) [17]. Fig. 2 shows the normalized unit-cell volume (V_p) as a function of chromium content. Within each of three compositional ranges, the $V_p(x)$ variation is monotonic. A drop of the volume value (−1.3%) is observed when crossing the boundary between the *R3c* phase range and the *Pnma* one, while no real jump in $V_p(x)$ can be stated at the *Pnma* - *C2/c* border. A similar compositional behaviour of the normalized perovskite unit-cell volume was observed in the $BiFe_{1-x}Sc_xO_3$ solid solutions, except for the fact that V_p in the Sc-containing system was an increasing function of x.

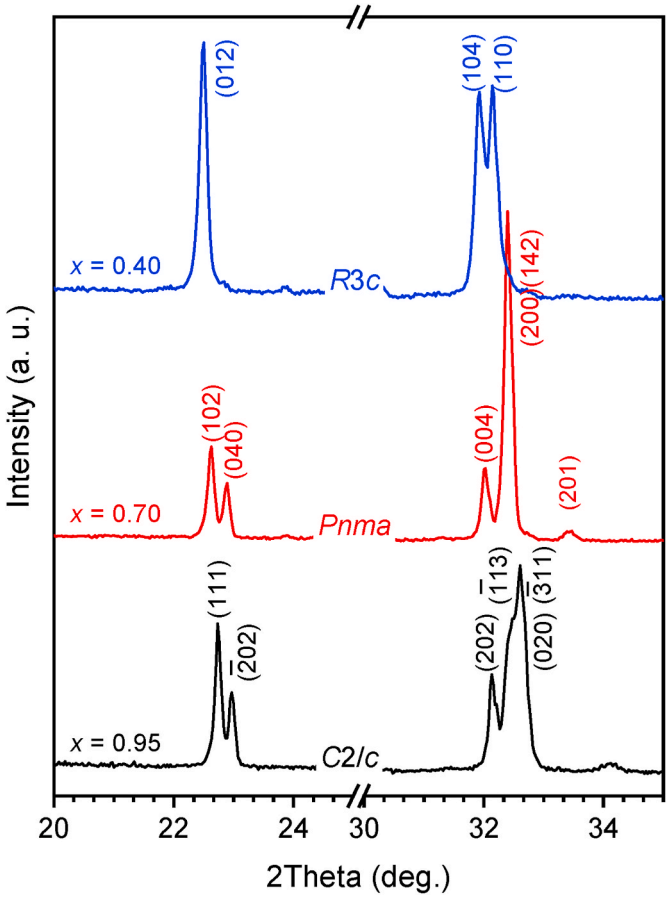

Fig. 1. XRD patterns of the as-prepared $BiFe_{1-x}Cr_xO_3$ samples synthesized under high pressure with the fundamental diffraction reflection indexed.

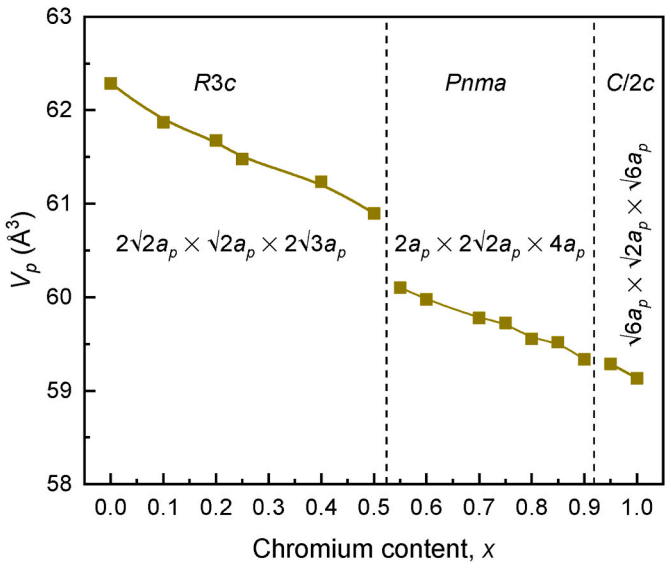

Fig. 2. The normalized unit-cell volume (V_p) of the $BiFe_{1-x}Cr_xO_3$ perovskite phases as a function of the chromium content (x) with the tentative borders of the phase ranges. The space groups and the superstructures are indicated (a_p is the pseudocubic primitive perovskite unit-cell parameter).

The compositional dependence of the lattice parameters and angles of the primitive perovskite unit-cell of the as-prepared $BiFe_{1-x}Cr_xO_3$ samples is shown in Fig. 3.

In the range of the rhombohedral phase isostructural to that of the parent $BiFeO_3$, the primitive perovskite cell demonstrates a trend to become cubic: the angle α_p increases towards 90° with increasing x (under the conditions $a_p = b_p = c_p$ and $\alpha_p = \beta_p = \gamma_p < 90^o$). Nevertheless, at $x \ge 0.55$, a smaller-volume pseudo-monoclinic unit cell ($a_p = c_p > b_p$, $\alpha_p = \gamma_p = 90^o$ and $\beta_p < 90^o$) is more favourable. Further increase of chromium content leads to a decrease of β_p. The a_p parameter progresses almost linearly, even across the range borders where the composition-driven phase transitions occur.

The thermal stability limits of the $BiFe_{1-x}Cr_xO_3$ perovskite phases stabilized under high pressure were estimated from the temperature *in situ* XRD study at ambient pressure. The thermal stability limit was defined as the temperature which is 50 K lower than that when the diffraction reflections of non-perovskite phase started to appear. It was found that perovskites phases are stable until 770-870 K with the stability temperature decreasing as chromium content is increased.

Microstructure of the $BiFe_{1-x}Cr_xO_3$ ceramics representing each structural range detected (rhombohedral, orthorhombic and monoclinic) were studied by SEM. It was found that the samples synthesized from the precursors prepared *via* sol-gel demonstrated smaller grains than those obtained from mixed oxides. All the studied samples displayed good densification and no visible porosity. Annealing of the samples at temperatures below their thermal stability limit was found to results in no microstructural change. Fig. 4 shows typical images of fractured surface of the $BiFe_{0.05}Cr_{0.95}O_3$ ceramics before and after annealing: no evident difference is seen.

It was observed that the average grain size trends to decrease with increasing chromium content (Fig. 5). The largest measured average

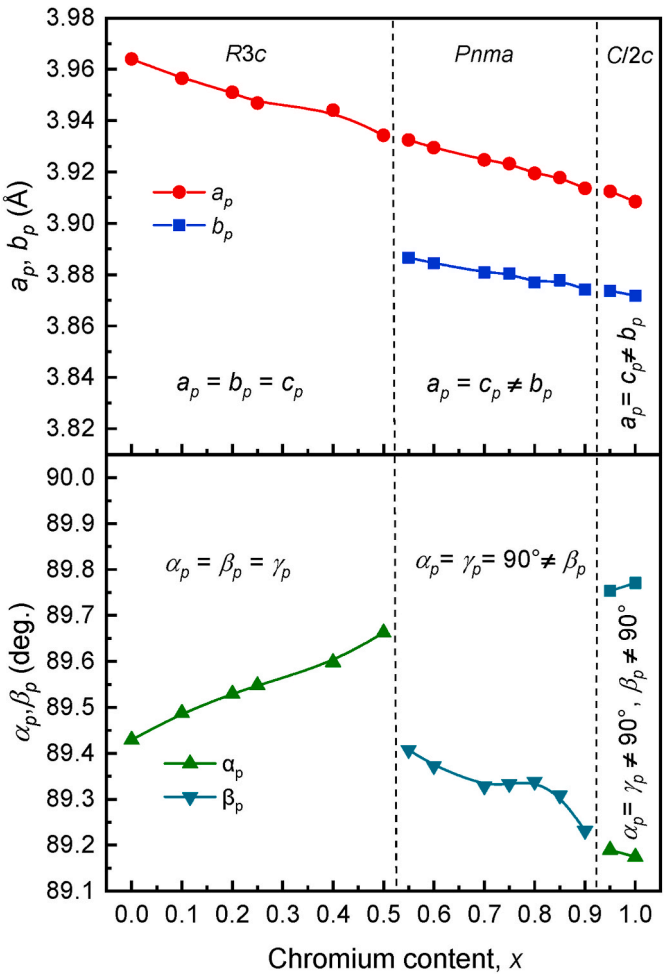

Fig. 3. The lattice parameters and angles of the primitive perovskite cell across the entire compositional range of the $BiFe_{1-x}Cr_xO_3$ series. The dashed lines indicate the tentative borders of the different phase ranges.

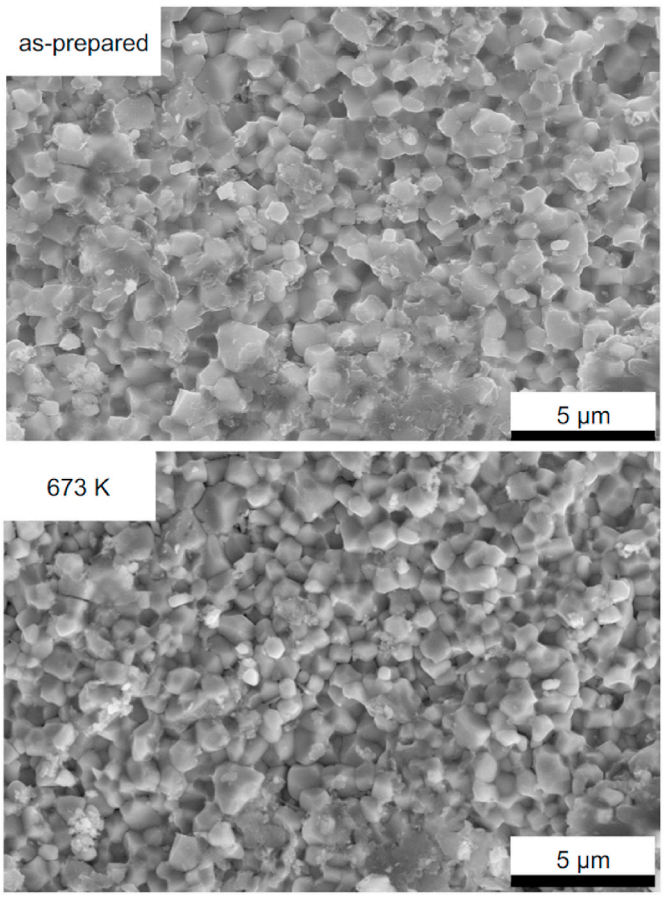

Fig. 4. SEM micrographs of $BiFe_{0.05}Cr_{0.95}O_3$ prepared from mixed oxides, before (top panel) and after annealing at 673 K for 2 h (bottom panel).

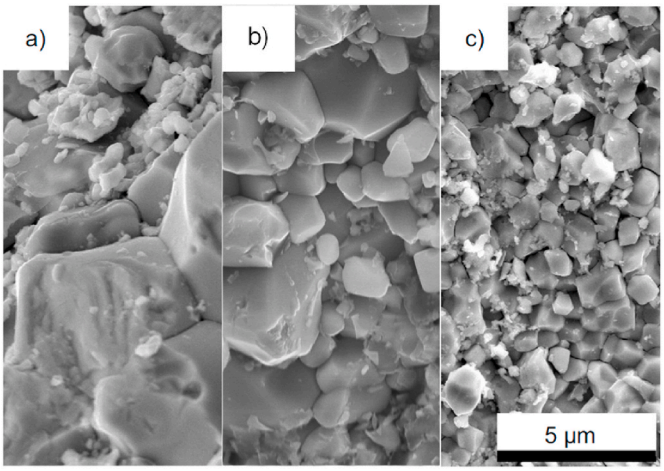

Fig. 5. SEM micrographs of the as-prepared samples: a) $BiFe_{0.90}Cr_{0.10}O_3$ (the average grain size of 7.99 μm) prepared using mixed-oxides method; b) $BiFe_{0.45}Cr_{0.55}O_3$ (3.94 μm) prepared via sol-gel route; c) $BiFe_{0.05}Cr_{0.95}O_3$ (1.70 μm) prepared via sol-gel route.

grain size of about 8 μm was detected in the $BiFe_{0.90}Cr_{0.10}O_3$ ceramics, while the $BiFe_{0.45}Cr_{0.55}O_3$ ceramics exhibited a bimodal grain size distribution with considerable fraction of large grains (above 3.5 μm).

The *in situ* XRD experiments confirmed a previously reported phase transition to a high-temperature orthorhombic phase [37]. Regardless of the structure of the perovskite phase of $BiFe_{1-x}Cr_xO_3$ before annealing (the rhombohedral, the antipolar orthorhombic or the monoclinic), increasing temperature was found to induce structural transformation into a non-polar orthorhombic modification (*Pnma*, $\sqrt{2}a_p \times 2a_p \times \sqrt{2}a_p$). Transformation occurred through a temperature range of phase coexistence (typically 10-20 K), which turned to be notably wider (60 K) in the vicinity of the compositional border ($0.50 \leq x \leq 0.55$) between the rhombohedral and the antipolar orthorhombic phases (Fig. 6). The transition temperature gradually decreased with increasing Cr content.

All the $BiFe_{1-x}Cr_xO_3$ compositions studied (except for $BiFe_{0.45}Cr_{0.55}O_3$) showed a reversible phase transition to the non-polar orthorhombic *Pnma* structure, with the volume expansion exhibiting identical trends both upon heating and cooling (Fig. 7).

The as-prepared antipolar *Pnma* polymorph of $BiFe_{0.45}Cr_{0.55}O_3$ was revealed to transform into the non-polar *Pnma* phase between 523 and 543 K upon heating followed by a transformation to the two-phase (*R3c* + antipolar *Pnma*) mixture at ~543 K upon cooling (Fig. 8).

The annealing stimulated transformation observed in $BiFe_{0.45}Cr_{0.55}O_3$ is an example of the *conversion polymorphism*, although incomplete. The *R3c* phase resulted from the annealing was found to have a smaller volume than that of the composition $BiFe_{0.50}Cr_{0.50}O_3$ and the initial (non-annealed) antipolar *Pnma* structure of $BiFe_{0.45}Cr_{0.55}O_3$.

3.2. Dielectric properties

The temperature dependence of the real and the imaginary parts of the complex dielectric permittivity of the $BiFe_{1-x}Cr_xO_3$ ceramics at 100 kHz is shown in Fig. 9. One can see gradual increase of both ε' and ε''

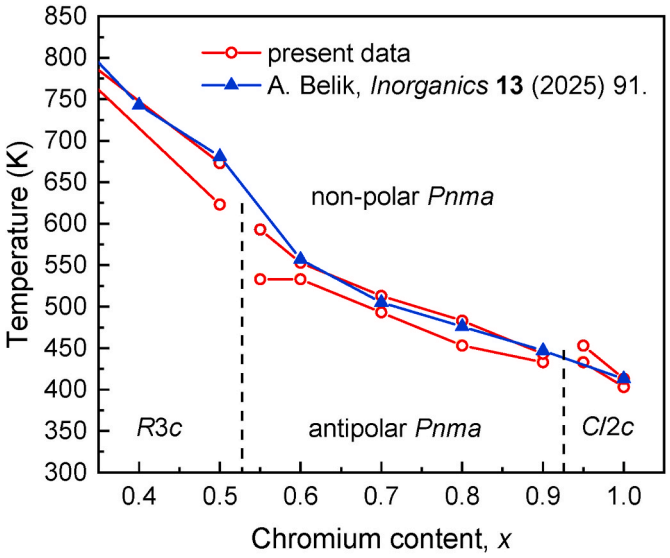

Fig. 6. The most representative part of the $BiFe_{1-x}Cr_xO_3$ phase diagram (upon heating). The transition temperature dependence reported by Belik [37] is shown for comparison.

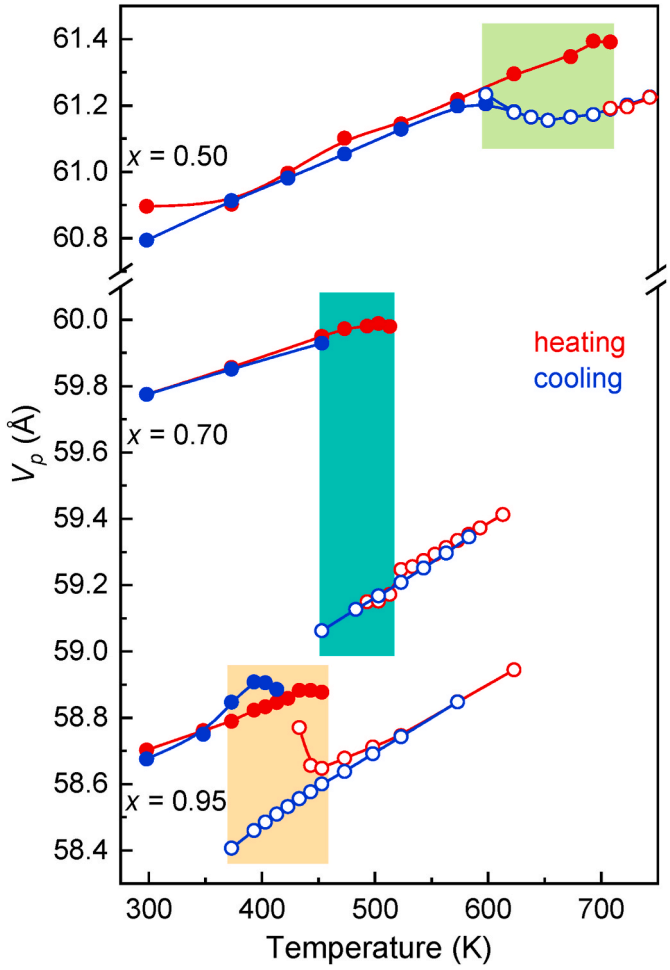

Fig. 7. Normalized primitive unit cell volume (V_p) of as-prepared $BiFe_{1-x}Cr_xO_3$ solid solutions as a function of temperature upon annealing. The shadow zones indicate the temperature ranges of phase coexistence.

with increasing temperature and the relative increment ($\Delta\varepsilon''/\Delta T$) of the

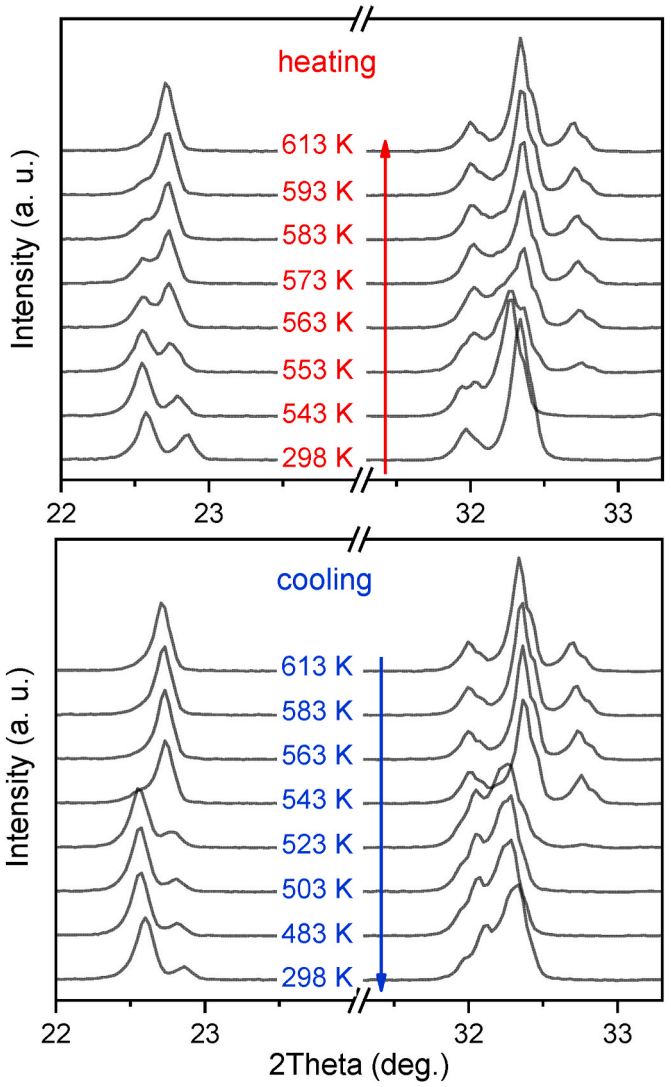

Fig. 8. Relevant ranges of the *in situ* XRD patterns of as-prepared $BiFe_{0.45}Cr_{0.55}O_3$ illustrating the irreversible antipolar *Pnma* → non-polar *Pnma* transformation upon heating (top panel) and the reversible non-polar *Pnma* → (antipolar *Pnma* + *R*3*c*) transition upon cooling (bottom panel).

imaginary part is considerably bigger than ($\Delta\varepsilon'/\Delta T$) at any temperature within the studied range of 200-500 K. Such a behaviour is typically associated with contribution of conductivity [33]. The oxide materials, which contain iron and chromium are expected to demonstrate high loss caused by the variable oxidation states (i.e., Fe^{3+} and Fe^{2+} as well as Cr^{3+} and Cr^{6+}) of these elements. Charge hopping between these states together with polarization of possible oxygen vacancies contribute to *intrinsic loss* of the $BiFe_{1-x}Cr_xO_3$ perovskites [36]. However, in case of materials prepared using high-pressure synthesis, the dielectric loss associated with the microstructure and residual stress (*extrinsic loss*) is certainly more considerable than intrinsic one. The room temperature value of $\tan\delta = \varepsilon''/\varepsilon'$ measured at 100 kHz in the high-pressure stabilized $BiFe_{1-x}Cr_xO_3$ ceramics with $x = 0.5$ reported by Wu et al. [36] and found in this study differ as 0.14 and 0.45, respectively. Resulting microstructure (grain size and size distribution, porosity, microcracks) as well as mechanical stress in the samples are determined not only by the synthesis conditions (pressure, temperature, dwell time) but also by the way how these conditions are realised; namely whether pressure was hydrostatic or not, what the heating & cooling rate was, how fast pressure was released *etc*. Therefore, microstructure-sensitive properties (in particular, dielectric properties) of high-pressure synthesized ceramics

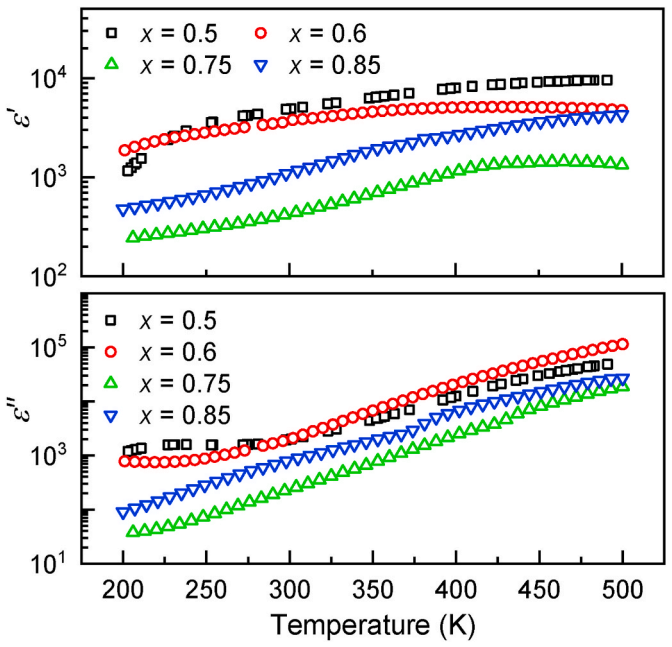

Fig. 9. Temperature dependence of the real part (top) and imaginary (bottom) parts of the complex dielectric permittivity of the $BiFe_{1-x}Cr_xO_3$ ceramics with different chromium content, *x*, at 100 kHz.

reported by different authors can be signally marked from each other.

Fig. 10 shows the real and imaginary parts of complex dielectric permittivity of the $BiFe_{1-x}Cr_xO_3$ ceramics at 250 K as a function of frequency. The Cole-Cole equation was used for fitting the dielectric spectra:

$$\varepsilon^* = \varepsilon' - i\varepsilon'' = \varepsilon_\infty + \frac{\Delta\varepsilon}{1+(i\omega\tau)^{1-\alpha}} - \frac{i\sigma}{\varepsilon_0\omega} \quad (1)$$

Here ε_∞ is permittivity at high frequency, $\Delta\varepsilon$ - dielectric strength of the relaxation, τ - mean Cole-Cole relaxation time, and α - Cole-Cole relaxation time distribution parameter. Solid lines in Fig. 10 represent the best fit. The dispersion maximum is seen to shift to higher frequencies as chromium content in the $BiFe_{1-x}Cr_xO_3$ system is increased, while the low-frequence conductivity remains almost unchanged.

The obtained temperature-dependent Cole-Cole parameters are presented in Figs. 11 and 12. The α parameter, which describes the width of the distribution of symmetric relaxation times was found to range from 0.2 to 0.3 (Fig. 11a). It means that the width of the relaxation distribution does not change within the error limits when increasing the temperature. It is seen from Fig. 11b that the dielectric constant at infinite frequency, ε_∞, of the $BiFe_{1-x}Cr_xO_3$ ceramics with $x = 0.5$ is about 250 while it is of order of 100 for other compositions studied. The temperature deviation from these values in the range of 200-300 K is below 10%. Fig. 11c shows the dielectric strengths of the $BiFe_{1-x}Cr_xO_3$ samples as a function of temperature. As known, dielectric strength in static dielectric constant describes the polarization. Therefore, notably higher values of ε_∞ and $\Delta\varepsilon$ observed in solid solution with $x = 0.5$ as compared with those of the compositions with $x = 0.6$, 0.75 and 0.85, are in good agreement with the theoretical predictions of exceptionally high-polarization in rhombohedral $BiFe_{0.5}Cr_{0.5}O_3$ [35].

Fig. 12 shows the temperature dependence of the mean relaxation time, obtained by fitting of the measured data using the Cole-Cole equation, expressed as $\ln[\tau]$ *versus* $1/T$. Activation energy (E_A) and the parameter (τ_0) for each composition studied were evaluated using the Arrhenius law $\tau = \tau_0 \exp(E_A/kT)$ and listed in Table 1.

One can see from Table 1 that the activation energy decreases, and the average relaxation time increases with increasing chromium content. This indicates that the Cr substitution results in lowering the energy barrier thereby facilitating the polarization relaxation process. As compared to other $BiFeO_3$-based multiferroics, the obtained activation energies (0.14-0.18 eV) are relatively low. For example, activation energy value measured in undoped bismuth ferrite ceramics at low temperatures and associated with $Fe^{2+} \leftrightarrow Fe^{3+}$ hopping was about 0.40 eV [39]. In doped systems, Ke et al. [40] reported the activation energy values of ~0.136 eV and ~0.239 eV attributed to electron jump processes, and a much higher one (~0.94 eV) associated with the migration of oxygen vacancies. Thus, the E_A values obtained for the $BiFe_{1-x}Cr_xO_3$ solid solutions indicate to the electron jump caused mechanism of the dielectric relaxation below room temperature.

The τ_0 values, ranging from 22.5 to 25.7 ps, are moderately high in

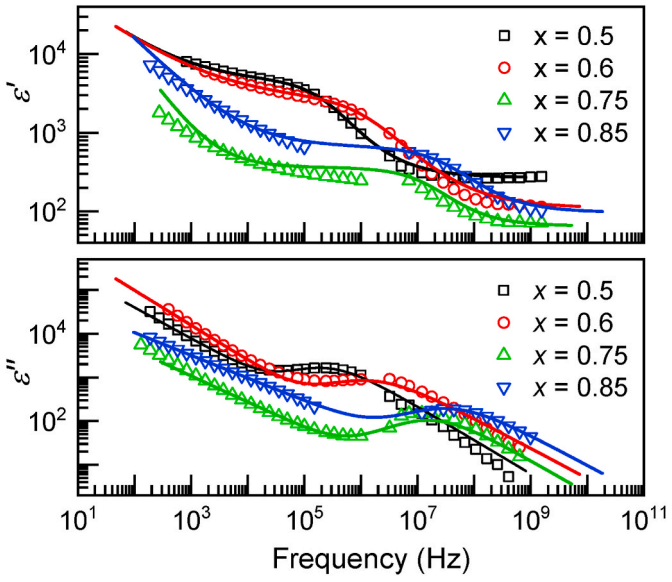

Fig. 10. Frequency dependence of the real (top) and imaginary (bottom) parts of the complex dielectric permittivity of $BiFe_{1-x}Cr_xO_3$ ceramics with different chromium content at 250 K. Solid lines represent fits using the Cole-Cole equation.

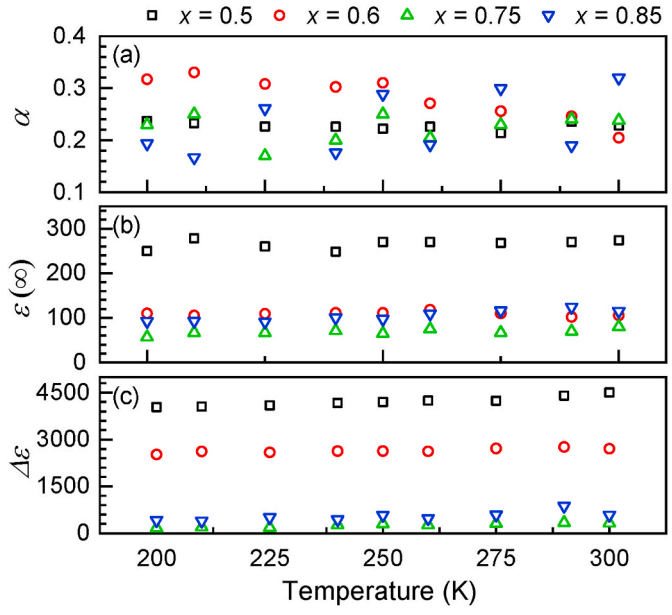

Fig. 11. Temperature dependence of the Cole-Cole parameters of the $BiFe_{1-x}Cr_xO_3$ ceramics: (a) relaxation time distribution parameter; (b) dielectric constant at high frequency, (c) dielectric strength of the relaxation.

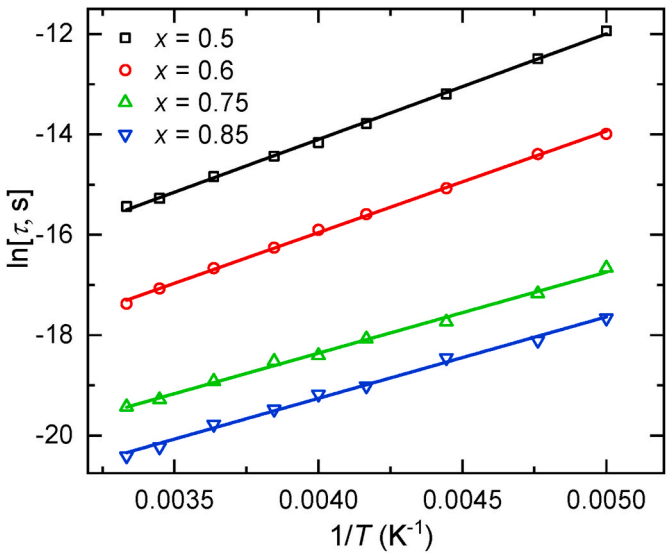

Fig. 12. Logarithm of the mean relaxation time (Cole-Cole) *versus* inverse temperature of the $BiFe_{1-x}Cr_xO_3$ ceramics. Solid lines represent fits using Arrhenius law.

comparison with undoped $BiFeO_3$, where τ_0 is typically reported to be below 20 ps. The observed growth of τ_0 with increasing chromium content is not strong although regular and reflects a slowdown of intrinsic relaxation dynamics. The nature of this effect is still unclear and requires a particular study using supplementary techniques.

The complex electric conductivity σ^* was calculated according to the relationship: $\sigma^* = i\varepsilon^*\varepsilon_0\omega$, where ω is the angular frequency and ε_0 is the dielectric permittivity of vacuum. The real part of complex conductivity was fitted with the Almond-West power law [41]:

$$\sigma(\omega) = \sigma_{DC} + A\omega^s \quad (2)$$

Here σ_{DC} is the DC conductivity and $A\omega^s$ is the AC conductivity.

Fig. 13 shows the $\ln(\sigma_{DC})$ *versus* $1/T$ dependences fitted with the Arrhenius law $\sigma_{DC} = \sigma_0\exp(E_A/kT)$, where σ_0 is the pre-exponential factor and E_A is the activation energy. The obtained E_A values are listed in Table 2.

As seen from Table 2, the activation energies associated with the $\sigma_{DC}(T)$ dependence of the $BiFe_{1-x}Cr_xO_3$ ceramics are in the range of 0.27-0.41 eV with the value increasing as chromium content is increased. The solid solution with $x = 0.85$ demonstrates the conductivity behaviour which is different in the temperature ranges of 300-376 K and 400-500 K (see Fig. 13). It corresponds to two distinct values of activation energy (0.414 and 0.274 eV) indicating to a coexistence of different conduction mechanisms. These E_A values are comparable to those reported for other doped $BiFeO_3$ ceramics. For example, Ca-doped $BiFeO_3$ shows activation energies in the range of 0.27-0.45 eV at room temperature, which is attributed to mixed p-type semiconduction and oxide-ion transport [42]. This suggests that the conductivity of the $BiFe_{1-x}Cr_xO_3$ ceramics is driven by a mixed mechanism. At medium chromium contents ($x = 0.50$-0.60), the relatively low E_A values indicate that electron hopping between Fe ions is likely to dominate. The higher values (~0.41 eV) found in solid solutions with $x = 0.75$ and 0.85 can mean that oxygen vacancy migration becomes more important. This is consistent with the results of Masó et al., [43] who reported oxygen vacancy-related conductivity associated with barriers of 0.4-0.6 eV in Ca-doped $BiFeO_3$ ceramics.

The temperature range where the activation energy of the $x = 0.85$ composition changes, namely 376-400 K is very close to the of range of the phase transition between two orthorhombic phases (see Fig. 6). Therefore, the E_A values of 0.414 and 0.274 eV can be attributed to the antipolar *Pnma* and the non-polar *Pnma* modifications of $BiFe_{0.15}Cr_{0.85}O_3$, respectively.

3.3. Magnetic behaviour

The magnetic properties of the representative compositions ($x = 0.4$, 0.55, 0.75, 0.8, 0.9, 0.95) starting with the composition with *R*3*c* structure and following the increase of the Cr content in the $BiFe_{1-x}Cr_xO_3$ solid solution system were studied as temperature- and field dependences of their magnetic moment. This range of compositions is complementary to the recently published magnetic data [37,44], giving insight into the magnetic behaviour with the possibility of the appearance of conversion polymorphism phenomena. As previously shown [45], undoped $BiCrO_3$ displays a spin-reorientation transition below the Néel temperature, and that behavior can be preserved for low Fe dopings [37]. Indeed, in our high-pressure synthesized ceramics with 5 mol% of Fe ($x = 0.95$), two anomalies were observed in the temperature

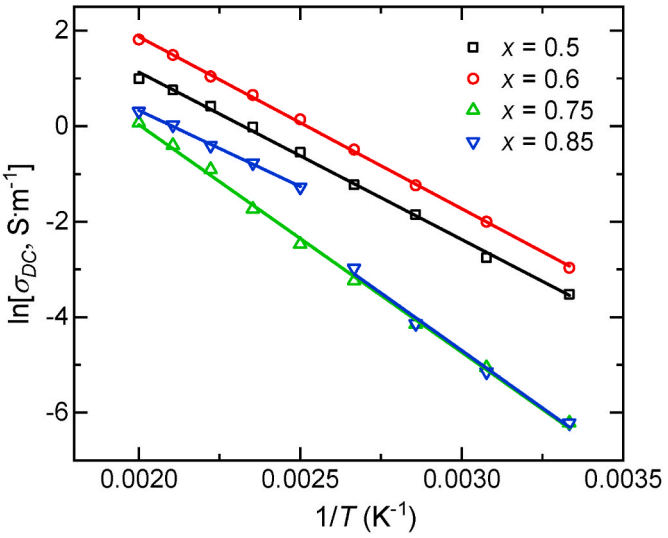

Fig. 13. Logarithm of σ_{DC} *versus* inverse temperature of the $BiFe_{1-x}Cr_xO_3$ ceramics. Solid lines represent a fit with the Arrhenius law.

Table 2
The activation energy values obtained from fitting of the temparature dependence of DC conductivity of the $BiFe_{1-x}Cr_xO_3$ ceramics using the Arrhenius law in the temperature range of 300-500 K.

Composition	$x = 0.5$	$x = 0.6$	$x = 0.75$	$x = 0.85$
E_A (eV)	0.302 ± 0.006	0.310 ± 0.003	0.410 ± 0.007	0.414 ± 0.026 **(300–376 K)** 0.274 ± 0.007 **(400–500 K)**

Table 1
Approximation parameters E_A and τ_0 obtained for the $BiFe_{1-x}Cr_xO_3$ ceramics studied using the Arrhenius law.

Composition	$x = 0.5$	$x = 0.6$	$x = 0.75$	$x = 0.85$
E_A (eV)	0.181 ± 0.002	0.174 ± 0.002	0.139 ± 0.003	0.139 ± 0.004
τ_0 (ps)	22.5 ± 0.1	24 ± 0.2	24.8 ± 0.2	25.7 ± 0.2

dependence of the M/H as shown in Fig. 14.

First, a small anomaly at 138 K and the onset of weak FM moment due to spin canting, detected as the difference between ZFC and FC response, is present. The second anomaly was observed at 93 K and assigned to spin-reorientation. Both transitions are clearly detectable also in the temperature dependence of the AC susceptibility shown in the inset of Fig. 14. Further increase of Fe content clearly yields a deviation from the magnetic behaviour of the undoped $BiCrO_3$: already in the composition with $x = 0.9$, the spin-reorientation transition is suppressed and the Néel temperature decreased to 85 K (Fig. 14). Another interesting phenomenon related to the presence of the magnetization reversal below the Néel temperature was observed in compositions with $x = 0.9$ and 0.8 (Fig. 14a and b, respectively). While the recent work of Belik [37] reports this behaviour for $x = 0.8$ only, it seems to appear in a wider range of the $BiFe_{1-x}Cr_xO_3$ solid solutions. Such magnetization reversal was previously observed in rare-earth-based $REFe_{1-x}Cr_xO_3$ solid solutions and explained by the competition of Dzyaloshinskii-Moriya (DM) interaction between Fe and Cr ions in the perovskite structure with the DM interaction within Cr–Cr and Fe–Fe pairs [46,47]. As a result, a compensation point exists between the weak FM magnetizations of Fe and Cr sublattices in solid solutions. The theoretical predictions for *RE* = Lu, Y suggest the occurrence of the magnetization reversal in the central part of the doping range $x \approx 0.4$-0.5 as a consequence of the relative magnitudes of the Fe–Fe and Cr–Cr isotropic exchange interactions [46]. In the case of $BiFe_{1-x}Cr_xO_3$, the compensation point seems to be shifted to a higher Cr concentration range and was not observed in our experiment in any composition with $x \leq 0.75$ (see also Fig. 15). This can be understood as a result of different exchange interaction magnitudes in the studied Bi-based perovskites in comparison with *RE*-based perovskites. For comparison, the Fe–Fe exchange interaction in $YFeO_3$ and $BiFeO_3$ is ≈16 K [46] and ≈75 K [48,49], respectively, while the difference in Cr–Cr exchange interactions is much smaller [46,50,51]. In addition, the ratio of the compensation point and the Néel temperature $T_{comp}/T_N = 0.59$ for the composition with $x = 0.8$ was found to be lower than $T_{comp}/T_N = 0.75$ predicted in $REFe_{1-x}Cr_xO_3$ [47] or 0.83 observed experimentally in $YFe_{0.5}Cr_{0.5}O_3$. While the evolution of T_N in solid solutions reflects the magnitude of Fe–Cr isotropic exchange interaction, T_{comp} depends on the Fe–Cr DM interaction. Thus, for the case of $BiFe_{1-x}Cr_xO_3$, such a model would require a particular approach with specific values of DM interactions taken into account.

Regarding the compositions with a higher Fe content, it was found that as x is decreased, T_N also increases from 116 K for $x = 0.75$ to about 320 K for $x = 0.4$ (Fig. 14b and 15a) driven by the much higher magnetic ordering temperature in the $BiFeO_3$ end member. The obtained $T_N(x)$ data are in a good agreement with the magnetic phase diagram of $BiFe_{1-x}Cr_xO_3$ presented in Ref. [37].

As mentioned before, a *conversion polymorphism* phenomenon was detected in $BiFe_{0.45}Cr_{0.55}O_3$. Annealing of this solid solution ($x = 0.55$)

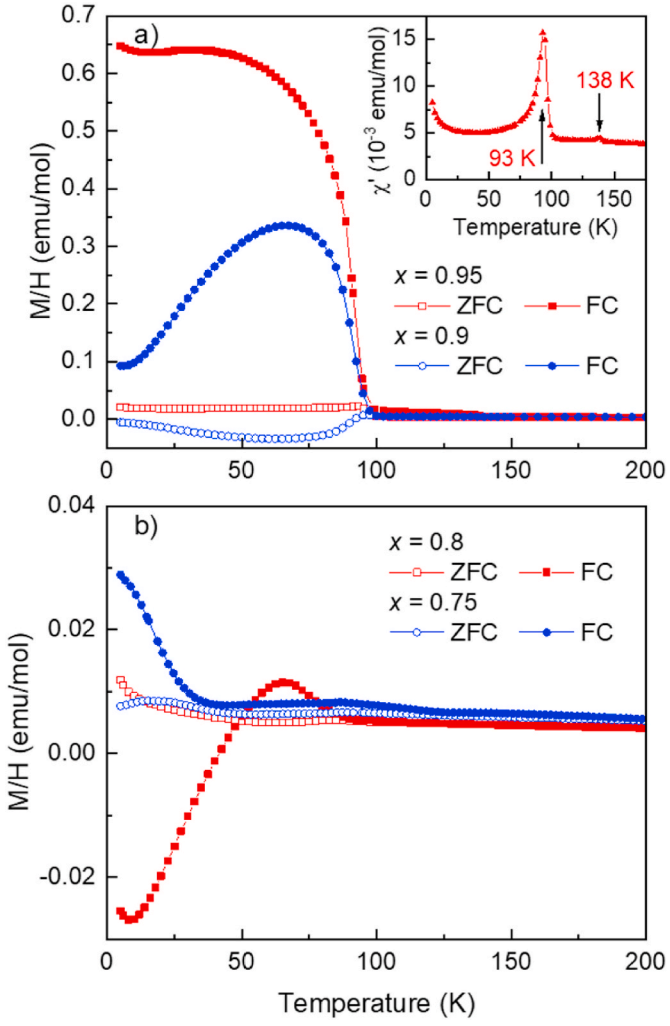

Fig. 14. The temperature dependence of *M/H* for $BiFe_{1-x}Cr_xO_3$ ceramics with (a) $x = 0.95$ and 0.9, (b) $x = 0.8$ and 0.75 obtained in the ZFC and FC regimes. The inset of (a) shows the real components of the AC susceptibility of the $x = 0.95$ composition measured with the excitation frequency of 8 Hz.

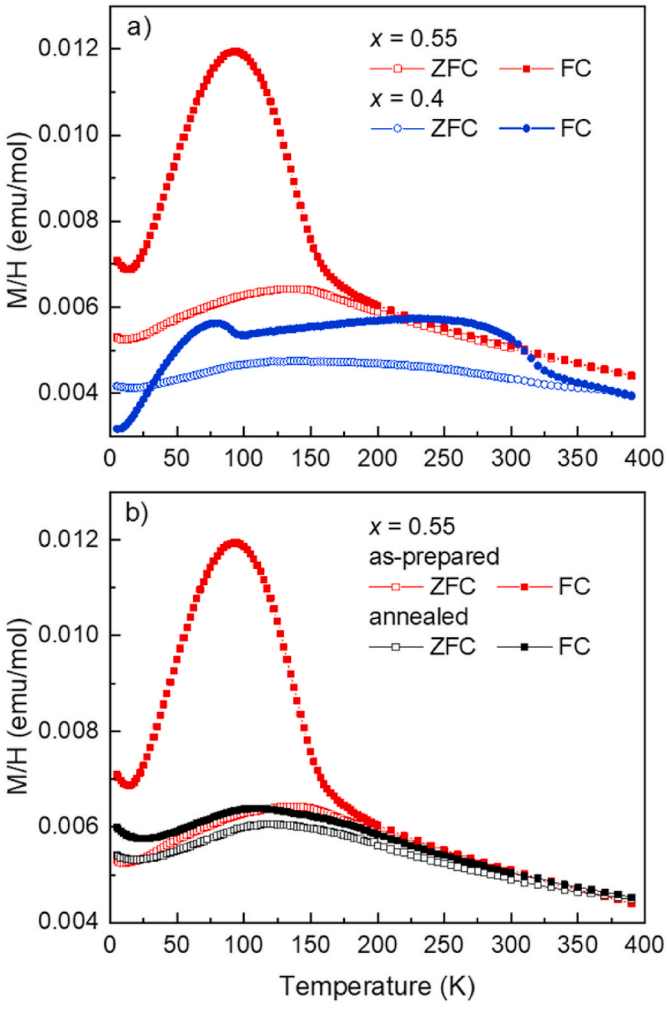

Fig. 15. a) The temperature dependence of *M/H* for $BiFe_{1-x}Cr_xO_3$ ceramics with $x = 0.55$ and 0.4. b) The temperature dependences of *M/H* for the as-prepared and the annealed $BiFe_{0.45}Cr_{0.55}O_3$ ceramics.

resulted in partial transformation of the as-prepared antipolar orthorhombic *Pnma* phase into the rhombohedral *R3c* one *via* formation of the high-temperature non-polar orthorhombic *Pnma* structure (Fig. 8). The influence of the conversion on the magnetic properties of the $BiFe_{0.45}Cr_{0.55}O_3$ ceramics was considered by comparison of the data measured before and after annealing in air at 720 K for 1 h. Two distinct maxima in the temperature dependence of *M/H* appeared instead of one in the as-prepared sample, as shown in Fig. 15b, and the observed weak FM moment was reduced as a signature of the contribution of the *R3c* phase, representative of the high Fe content perovskite with incommensurate AFM ordering.

For the $x = 0.4$ composition, whose structure symmetry is *R3c* both before and after annealing, two anomalies in the *M/H versus T* dependence were observed (Fig. 15a), namely one at $T_N \approx 320$ K and an additional sudden change in magnetic moment at 97 K. The lower-temperature anomaly might be evidence of the subsequent magnetic transition at T_m from the incommensurate AFM phase into another magnetic phase, perhaps the collinear AFM one, as that suggested in Fe-rich solid solutions of the systems $BiFe_{1-x}Sc_xO_3$ [20,52] and $BiFe_{1-x}[Zn_{0.5}Ti_{0.5}]_xO_3$ [53,54].

A reduction of the weak FM moment induced by the canted AFM moments was also observed in magnetization loops measured in magnetic fields up to 70 kOe at 5 K (Fig. S4). Once the spin-reorientation transition observed in $BiFe_{1-x}Cr_xO_3$ with $x = 0.95$ was suppressed by increasing Fe content, the coercivity was decreased with decreasing *x*, and magnetization curves obtained a more linear behavior in the full field range. The annealing, which results in partial *conversion polymorphism* in the $x = 0.55$ composition, leads to a similar effect as shown in Fig. S5. While the small coercivity is basically unchanged, the total magnetic moment is reduced, and a linear contribution to the field dependence of magnetization is more dominant, reminiscent of the behavior of high Fe content of $BiFe_{1-x}Sc_xO_3$ [52] or pure $BiFeO_3$.

4. Conclusions

Room-temperature compositional ranges of the as-prepared perovskite phases in the $BiFe_{1-x}Cr_xO_3$ solid solution system synthesized under high pressure have been refined. The solid solutions with composition from the range of $0 \leq x \leq 0.50$ crystallize in the rhombohedral *R3c* phase isostructural to the $BiFeO_3$ end member. The solid solutions from the range of $0.55 \leq x \leq 0.90$ are orthorhombic with the antipolar *Pnma* structure, while those from the range of $0.95 \leq x \leq 1$ are monoclinic with the same *C2/c* structure as that in the high-pressure stabilized $BiCrO_3$. No compositional ranges with phase coexistence have been detected. The compositional dependence of the normalized unit-cell volume is monotonic with the only jump (−1.3%) observed when crossing the border between the *R3c* phase range and the *Pnma* one.

In the $BiFe_{1-x}Cr_xO_3$ solid solutions from the range of $0.50 \leq x \leq 1$, regardless of the structure of the perovskite phase before annealing (the rhombohedral, the antipolar orthorhombic or the monoclinic), increasing temperature induces a reversible phase transition into a non-polar orthorhombic *Pnma* modification. The only case of temperature-induced irreversible transformation was observed in solid solution with composition of $x = 0.55$: the as-prepared antipolar *Pnma* polymorph of $BiFe_{0.45}Cr_{0.55}O_3$ transforms into the non-polar *Pnma* phase upon heating followed by a transformation to the two-phase (*R3c* + antipolar *Pnma*) mixture upon cooling.

Below 300 K, dielectric behaviour of the $BiFe_{1-x}Cr_xO_3$ ceramics is governed by relaxation dynamics described by the Cole-Cole model with the relaxation time distribution parameter α in the range of 0.2-0.3. Activation energy of the process estimated using the Arrhenius law decreases from 0.18 to 0.14 eV as the chromium content is increased from 50 to 85 mol%. Above 300 K, the $BiFe_{1-x}Cr_xO_3$ ceramics show electrical conductivity, which rises with temperature. Conductivity is characterized by activation energy values, which increase from 0.27 to 0.41 eV with increasing chromium content. This reflects a crossover in the dominant contribution to the conductivity from the $Fe^{2+} \leftrightarrow Fe^{3+}$ electron hopping in the compositions with $x = 0.5$ and 0.6 to the oxygen vacancy migration in those with $x = 0.75$ and 0.85. In the $BiFe_{0.15}Cr_{0.85}O_3$ solid solution, a sudden change of the conductivity-related activation energy from 0.414 to 0.274 eV within the interval of 376 to 400 K was observed and associated with phase transition from the antipolar *Pnma* phase to the non-polar *Pnma* modification.

The compositional behaviour of the Néel temperature of the $BiFe_{1-x}Cr_xO_3$ solid solutions studied is non-monotonic, with minimal $T_N(x)$ values detected in the *x* range of 0.8-0.9. Similar to the $BiCrO_3$ end member, the composition with 5 mol% of iron substitution demonstrates a spin re-orientation transition. The temperature of this transition in $BiFe_{0.05}Cr_{0.95}O_3$ is lower than that in bismuth chromate; in $BiFe_{0.10}Cr_{0.90}O_3$, a spin re-orientation is entirely suppressed. In the compositions with $x = 0.9$ and 0.8, a magnetization reversal effect below the Néel temperature was observed.

Annealed-stimulated irreversible phase transformation in the $BiFe_{0.45}Cr_{0.55}O_3$ solid solution was found to result in the appearance of two maxima in the temperature dependence of magnetic moment, corresponding to each of the structural phases in the annealed sample (rhombohedral *R3c* and antipolar orthorhombic *Pnma*).

In the $BiFe_{0.60}Cr_{0.40}O_3$ ceramics, an anomaly in the temperature-dependent magnetic behavior below T_N was observed, indicating to possible transition to the AFM collinear magnetic state.

CRediT authorship contribution statement

A.N. Salak: Validation, Supervision, Resources, Project administration, Investigation, Formal analysis, Conceptualization. **J.P. Cardoso:** Writing – original draft, Investigation, Formal analysis, Data curation. **D.D. Khalyavin:** Writing – review & editing, Investigation, Formal analysis, Conceptualization. **A.V. Pushkarev:** Methodology, Investigation, Data curation. **Yu.V. Radyush:** Investigation, Formal analysis, Data curation. **N.M. Olekhnovich:** Supervision, Resources, Methodology, Formal analysis, Conceptualization. **E.L. Fertman:** Validation, Resources, Formal analysis, Data curation. **A.V. Fedorchenko:** Visualization, Validation, Investigation, Formal analysis, Data curation. **D. Sokol:** Investigation, Formal analysis, Data curation. **E. Palaimienė:** Visualization, Investigation, Formal analysis, Data curation. **J. Banys:** Supervision, Project administration, Funding acquisition, Conceptualization. **S. Salamon:** Methodology, Investigation, Formal analysis, Data curation. **H. Wende:** Supervision, Project administration, Methodology, Funding acquisition, Conceptualization. **A. Feher:** Validation, Supervision, Resources, Funding acquisition, Formal analysis, Conceptualization. **E. Čižmár:** Writing – review & editing, Visualization, Supervision, Resources, Methodology, Formal analysis, Data curation, Conceptualization.

Declaration of competing interest

The authors declare that they have no known competing financial interests or personal relationships that could have appeared to influence the work reported in this paper.

Acknowledgements

This work was supported by project TUMOCS (2015-2018). This project has received funding from the European Union's Horizon 2020 research and innovation programme under the Marie Skłodowska-Curie grant agreement No 645660. The authors also acknowledge financial support of the bilateral Slovakia-Belarus project through grants APVV-SK-BY-RD-19-0008 and T20SLKG-001, respectively. Additional support was provided by the Slovak Research and Development Agency through project No. APVV-22-0172 and by the German Research Foundation (DFG) via the CRC/TRR 247 (Project-ID 388390466, subproject B02). The research done in the University of Aveiro was

supported by the project CICECO - Aveiro Institute of Materials, UID/50011/2025 (DOI 10.54499/UID/50011/2025) & LA/P/0006/2020 (DOI 10.54499/LA/P/0006/2020), financed by national funds through the FCT/MCTES (PIDDAC).

Appendix A. Supplementary data

Supplementary data to this article can be found online at https://doi.org/10.1016/j.jpcs.2026.113621.

Data availability

Data will be made available on request.

References

[1] I. Sosnowska, T. Peterlin-Neumaier, E. Steichele, Spiral magnetic ordering in bismuth ferrite, J. Phys. C Solid State Phys. 15 (1982) 4835–4846.
[2] I. Sosnowska, A.K. Zvezdin, Origin of the long period magnetic ordering in $BiFeO_3$, J. Magn. Magn Mater. 140–144 (1995) 167–168.
[3] YuF. Popov, A.M. Kadomtseva, G.P. Vorob'ev, A.K. Zvezdin, Discovery of the linear magnetoelectric effect in magnetic ferroelectric $BiFeO_3$ in a strong magnetic field, Ferroelectrics 162 (1994) 135–140.
[4] C.H. Yang, D. Kan, I. Takeuchi, V. Nagarajan, J. Seidel, Doping $BiFeO_3$: approaches and enhanced functionality, Phys. Chem. Chem. Phys. 14 (2012) 15953–15962.
[5] D.C. Arnold, Composition-driven structural phase transitions in rare-earth-doped $BiFeO_3$ ceramics: a review, IEEE Trans. Ultrason. Ferroelectrics Freq. Control 62 (2015) 62–82.
[6] J. Gebhardt, A.M. Rappe, Doping of $BiFeO_3$: a comprehensive study on substitutional doping, Phys. Rev. B 98 (2018) 125202.
[7] M. Azuma, H. Kanda, A.A. Belik, Y. Shimakawa, M. Takano, Magnetic and structural properties of $BiFe_{1-x}Mn_xO_3$, J. Magn. Magn Mater. 310 (2007) 1177–1179.
[8] P. Mandal, A. Sundaresan, C.N.R. Rao, A. Iyo, P.M. Shirage, Y. Tanaka, C. Simon, V. Pralong, O.I. Lebedev, V. Caignaert, B. Raveau, Temperature-induced magnetization reversal in $BiFe_{0.5}Mn_{0.5}O_3$ synthesized at high pressure, Phys. Rev. B 82 (2010) 100416.
[9] L. Pálová, P. Chandra, K.M. Rabe, Magnetostructural effect in the multiferroic $BiFeO_3$-$BiMnO_3$ checkerboard from first principles, Phys. Rev. Lett. 104 (2010) 037202.
[10] A.A. Belik, Origin of magnetization reversal and exchange bias phenomena in solid solutions of $BiFeO_3$-$BiMnO_3$: intrinsic or extrinsic? Inorg. Chem. 52 (2013) 2015–2021.
[11] D. Delmonte, F. Mezzadri, E. Gilioli, M. Solzi, G. Calestani, F. Bolzoni, R. Cabassi, Poling-written ferroelectricity in bulk multiferroic double-perovskite $BiFe_{0.5}Mn_{0.5}O_3$, Inorg. Chem. 55 (2016) 6308–6314.
[12] F. Sugawara, S. Iida, Magnetic properties and crystal distortions of $BiMnO_3$ and $BiCrO_3$, J. Phys. Soc. Japan 25 (6) (1968) 1553–1558.
[13] S.M. Selbach, T. Tybell, M.A. Einarsrud, T. Grande, Structure and properties of multiferroic oxygen hyperstoichiometric $BiFe_{1-x}Mn_xO_{3+\delta}$, Chem. Mater. 21 (2009) 5176–5186.
[14] A. Ianculescu, F.P. Gheorghiu, P. Postolache, O. Oprea, L. Mitoseriu, The role of doping on the structural and functional properties of $BiFe_{1-x}Mn_xO_3$ magnetoelectric ceramics, J. Alloys Compd. 504 (2010) 420–426.
[15] A.A. Belik, A.M. Abakumov, A.A. Tsirlin, J. Hadermann, J. Kim, G.V. Tendeloo, E. Takayama-Muromachi, Structure and magnetic properties of $BiFe_{0.75}Mn_{0.25}O_3$ perovskite prepared at ambient and high pressure, Chem. Mater. 23 (2011) 4505–4514.
[16] A.A. Belik, S. Iikubo, T. Yokosawa, K. Kodama, N. Igawa, S. Shamoto, M. Azuma, M. Takano, K. Kimoto, Y. Matsui, E. Takayama-Muromachi, Origin of the monoclinic-to-monoclinic phase transition and evidence for the centrosymmetric crystal structure of $BiMnO_3$, J. Am. Chem. Soc. 129 (2007) 971–977.
[17] A.N. Salak, D.D. Khalyavin, A.V. Pushkarev, YuV. Radyush, N.M. Olekhnovich, A. D. Shilin, V.V. Rubanik, Phase formation in the (1-*y*)$BiFeO_3$-*y*$BiScO_3$ system under ambient and high pressure, J. Solid State Chem. 247 (2017) 90–96.
[18] D.D. Khalyavin, A.N. Salak, N.M. Olekhnovich, A.V. Pushkarev, YuV. Radyush, P. Manuel, I.P. Raevski, M.L. Zheludkevich, M.G.S. Ferreira, Polar and antipolar polymorphs of metastable perovskite $BiFe_{0.5}Sc_{0.5}O_3$, Phys. Rev. B 89 (17) (2014) 174414.
[19] A.N. Salak, D.D. Khalyavin, E. Eardley, N.M. Olekhnovich, A.V. Pushkarev, YuV. Radyush, A.D. Shilin, V.V. Rubanik, Temperature-induced reversible and irreversible transitions between metastable perovskite phases in the $BiFe_{1-y}Sc_yO_3$ solid solutions, Crystals 8 (2018) 91–101.
[20] D.D. Khalyavin, A.N. Salak, E.L. Fertman, O.V. Kotlyar, E. Eardley, N. M. Olekhnovich, A.V. Pushkarev, YuV. Radyush, A.V. Fedorchenko, V.A. Desnenko, P. Manuel, L. Ding, E. Čižmár, A. Feher, The phenomenon of conversion polymorphism in Bi-containing metastable perovskites, Chem. Commun. 55 (2019) 4683–4686.
[21] C.V. Colin, A.G. Pérez, P. Bordet, C. Goujon, C. Darie, Symmetry adapted analysis of the magnetic and structural phase diagram of $Bi_{1-x}Y_xCrO_3$, Phys. Rev. B 85 (2012) 224103.
[22] A.A. Belik, Magnetic properties of solid solutions between $BiCrO_3$ and $BiGaO_3$ with perovskite structures, Sci. Technol. Adv. Mater. 16 (2015) 26003.
[23] C. Darie, C. Goujon, M. Bacia, H. Klein, P. Toulemonde, P. Bordet, E. Suard, Magnetic and crystal structures of $BiCrO_3$, Solid State Sci. 12 (2010) 660–664.
[24] J.P. Cardoso, D. Delmonte, E. Gilioli, E.L. Fertman, A.V. Fedorchenko, V. V. Shvartsman, V. Paukšta, R. Grigalaitis, J. Banys, D.D. Khalyavin, J.M. Vieira, A. N. Salak, Phase transitions in the metastable perovskite multiferroics $BiCrO_3$ and $BiCr_{0.9}Sc_{0.1}O_3$: a comparative study, Inorg. Chem. 59 (2020) 8727–8735.
[25] D. Behr, D. Delmonte, E. Gilioli, D.D. Khalyavin, R.D. Johnson, Weak ferromagnetism and spin reorientation in antiferroelectric $BiCrO_3$, Phys. Rev. B 106 (2022) 024416.
[26] B.C. Luo, C.L. Chen, K.X. Jin, Low temperature properties of multiferroic $BiFe_{0.9}Cr_{0.1}O_3$ compound, Solid State Commun. 151 (2011) 712–715.
[27] B.R. McBride, J. Lieschke, A. Berlie, D.L. Cortie, H.Y. Playford, T. Lu, N. Narayanan, R.L. Withers, D. Yu, Y. Liu, Study of the B-site ion behaviour in the multiferroic perovskite bismuth iron chromium oxide, J. Appl. Phys. 123 (2018) 154104.
[28] M.R. Suchomel, C. Thomas, M. Allix, M. Rosseinsky, A. Fogg, M. Thomas, High pressure bulk synthesis and characterization of the predicted multiferroic $Bi(Fe_{1/2}Cr_{1/2})O_3$, Appl. Phys. Lett. 90 (2007) 2–5.
[29] V.S. Pokatilov, V.S. Rusakov, A.S. Sigov, A.A. Belik, Mössbauer studies of multiferroics $BiFe_{1-x}Cr_xO_3$ (x = 0-0.20), Phys. Solid State 59 (2017) 1558–1564.
[30] I.P. Raevski, S.P. Kubrin, A.V. Pushkarev, N.M. Olekhnovich, YuV. Radyush, V. V. Titov, M.A. Malitskaya, S.I. Raevskaya, H. Chen, The effect of Cr substitution for Fe on the structure and magnetic properties of $BiFeO_3$ multiferroic, Ferroelectrics 525 (2018) 1–10.
[31] V.S. Rusakov, V.S. Pokatilov, A.S. Sigov, A.A. Belik, M.E. Matsnev, Changes in the magnetic structure of multiferroic $BiFe_{0.80}Cr_{0.20}O_3$ with temperature, Phys. Solid State 61 (2019) 1030–1036.
[32] S.P. Kubrin, I.P. Raevski, N.M. Olekhnovich, A.V. Pushkarev, Y.V. Radyush, V. V. Titov, M.A. Malitskaya, G.R. Li, S.I. Raevskaya, Mössbauer study of the effect of cation substitutions on the magnetic phase transitions in $BiFe_{1-x}Cr_xO_3$ and (1–*x*) $BiFeO_3$–*x*$PbFe_{0.5}Sb_{0.5}O_3$ solid solutions, Crystallogr. Rep. 65 (2020) 338–342.
[33] E. Palaimiene, V. Gribauskaite, J. Banys, A.V. Pushkarev, Y.V. Radyush, N. M. Olekhnovich, J.P.V. Cardoso, A.N. Salak, Dielectric characterization of the $BiFe_{0.5}Cr_{0.5}O_3$ ceramics, Lith. J. Phys. 62 (2022) 206–211.
[34] C. Himcinschi, F. Drechsler, D.S. Walch, A. Bhatnagar, A.A. Belik, J. Kortus, Unexpected phonon behaviour in $BiFe_xCr_{1-x}O_3$, a material system different from its $BiFeO_3$ and $BiCrO_3$ parents, Nanomaterials 12 (2022) 1607.
[35] P. Baettig, C. Ederer, N.A. Spaldin, First principles study of the multiferroics $BiFeO_3$, Bi_2FeCrO_6, and $BiCrO_3$: structure, polarization, and magnetic ordering temperature, Phys. Rev. B 72 (2005) 214105.
[36] H. Wu, Z. Pei, W. Xia, Y. Lu, K. Leng, X. Zhu, Structural, magnetic, dielectric and optical properties of double perovskite Bi_2FeCrO_6 ceramics synthesized under high pressure, J. Alloys Compd. 819 (2020) 153007.
[37] A.A. Belik, The conversion polymorphism of perovskite phases in the $BiCrO_3$-$BiFeO_3$ system, Inorganics 13 (2025) 91.
[38] J. Rodriguez-Carvajal, Recent advances in magnetic structure determination by neutron powder diffraction, Phys. B Phys. Condens. Matter 192 (1993) 55–69.
[39] E. Markiewicz, B. Hilczer, M. Błaszyk, A. Pietraszko, E. Talik, Dielectric properties of $BiFeO_3$ ceramics obtained from mechanochemically synthesized nanopowders, J. Electroceram. 27 (2011) 154–161.
[40] Q. Ke, X. Lou, Y. Wang, J. Wang, Oxygen-vacancy-related relaxation and scaling behaviors of $Bi_{0.9}La_{0.1}Fe_{0.98}Mg_{0.02}O_3$ ferroelectric thin films, Phys. Rev. B 82 (2010) 024102.
[41] D. Almond, G.K. Duncan, A.R. West, Solid State Ionics 8 (1983) 159.
[42] N. Masó, A.R. West, Electrical properties of Ca-doped $BiFeO_3$ ceramics: prom p-type semiconduction to oxide-ion conduction, Chem. Mater. 24 (2012) 2127–2132.
[43] N. Masó, H. Beltrán, M. Prades, E. Cordoncillo, A.R. West, Field-enhanced bulk conductivity and resistive-switching in Ca-doped $BiFeO_3$ ceramics, Phys. Chem. Chem. Phys. 16 (2014) 19408–19416.
[44] S.S. Arafat, Structural transition and magnetic properties of high Cr-doped $BiFeO_3$ ceramic, Cerâmica 66 (2020) 114–118.
[45] A.A. Belik, N. Tsujii, H. Suzuki, E. Takayama-Muromachi, Magnetic properties of bulk $BiCrO_3$ studied with dc and ac magnetization and specific heat, Inorg. Chem. 46 (2007) 8746–8751.
[46] N. Dasari, P. Mandal, A. Sundaresan, N.S. Vidhyadhiraja, Weak ferromagnetism and magnetization reversal in $YFe_{1-x}Cr_xO_3$, Europhys. Lett. 99 (2012) 17008.
[47] O.V. Billoni, F. Pomiro, S.A. Cannas, C. Martin, A. Maignan, R.E. Carbonio, Magnetization reversal in mixed ferrite-chromite perovskites with non magnetic cation on the A-site, J. Phys. Condens. Matter 28 (2016) 476003.
[48] M. Matsuda, R.S. Fishman, T. Hong, C. Lee, T. Ushiyama, Y. Yanagisawa, Y. Tomioka, T. Ito, Magnetic dispersion and anisotropy in multiferroic $BiFeO_3$, Phys. Rev. Lett. 109 (2012) 067205.
[49] C. Xu, B. Xu, B. Dupé, L. Bellaiche, Magnetic interactions in $BiFeO_3$: a first-principles study, Phys. Rev. B 99 (2019) 104420.
[50] B.S. Araújo, A.M. Arévalo-López, C.C. Santos, J.P. Attfield, C.W.A. Paschoal, A. P. Ayala, Spin–phonon coupling in monoclinic $BiCrO_3$, J. Appl. Phys. 127 (2020) 114102.
[51] Y. Xu, X. Hao, J. Meng, D. Zhou, F. Gao, Electronic and magnetic properties of the monoclinic phase $BiCrO_3$ from first-principles studies, J. Phys. Condens. Matter 21 (2009) 236006.
[52] E.L. Fertman, A.V. Fedorchenko, E. Čižmár, S. Vorobiov, A. Feher, Y.V. Radyush, A. V. Pushkarev, N.M. Olekhnovich, A. Stanulis, A.R. Barron, D.D. Khalyavin, A.

N. Salak, Magnetic diagram of the high-pressure stabilized multiferroic perovskites of the $BiFe_{1-y}Sc_yO_3$ series, Crystals 10 (2020) 950.

[53] E. Ćižmár, S. Vorobiov, A. Kliuikov, Y.V. Radyush, A.V. Pushkarev, N. M. Olekhnovich, J.P. Cardoso, A.N. Salak, A. Feher, Structural and magnetic phase transitions in the Fe-rich compositional range of the multiferroic $BiFe_{1-x}[Zn_{0.5}Ti_{0.5}]_xO_3$ perovskites, Integrated Ferroelectrics Int. J. 220 (2021) 1–8.

[54] A.N. Salak, J.P.V. Cardoso, V.M. Vieira, V.V. Shvartsman, D.D. Khalyavin, E. L. Fertman, A.V. Fedorchenko, A.V. Pushkarev, Y.V. Radyush, N.M. Olekhnovich, R. Tarasenko, A. Feher, E. Ćižmár, Magnetic behaviour of perovskite compositions derived from $BiFeO_3$, Magnetochemistry 7 (2021) 151.